ARCADA

THIS IS A SELF-ARCHIVED VERSION OF THE ORIGINAL PUBLICATION

The self-archived version is a publisher‘s pdf of the original publication. NB. The self-archived version may differ from the original in pagination, typographical details and illustrations.

To cite this, use the original publication:

Gebrehiwot, S.Z., Espinosa-Leal, L., Andersson, M., & Remes, H. (2023). On the Short-Term Creep and Recovery Behaviors of Injection Molded and Additive-Manufactured Tough

DOI: https://doi.org/10.1007/s11665-023-08278-6

Permanent link to the self-archived copy:

All material supplied via Arcada’s self-archived publications collection in Theseus repository is protected by copyright laws. Use of all or part of any of the repository collections is permitted only for personal non-commercial, research or educational purposes in digital and print form. You must obtain permission for any other use.

JAN-MAGNUS JANSSONS PLATS 1, FIN-00550 HELSINGFORS, TEL: +358 (0)20 769 9699 FAX: +358 (0)20 769 9622 www.arcada.fi

JMEPEG
https://doi.org/10.1007/s11665-023-08278-6
©The Author(s)
1059-9495/$19.00

TECHNICAL ARTICLE

On the Short-Term Creep and Recovery Behaviors of Injection Molded and Additive-Manufactured Tough Polylactic Acid Polymer

Silas Z. Gebrehiwot, Leonardo Espinosa-Leal, Mirja Andersson, and Heikki Remes

Submitted: 28 September 2022 / Revised: 17 April 2023 / Accepted: 29 April 2023

The creep and recovery behaviors of a tough polylactic acid polymer are investigated experimentally and theoretically. We studied the influence of manufacturing methods and parameters on the viscoelastic responses. Experimental comparisons were carried out on 13 different samples manufactured using fused deposition modeling (FDM) and injection molding methods. The sample variations in the FDM were based on four infill densities (70-100%) and 3 infill directions $(0°, 45°, 90°)$. Theoretically, the Burgers and Weibull's models are used to predict the creep and recovery responses of the samples. Our experimental findings suggest that the injection-molded samples perform better in creep for most of the cases. However, at higher stress loadings, the 90 and 100% infill density samples showed excellent creep resistance behaviors at the 90° infill direction. On the other hand, the theoretical creep and recovery predictions were based on the nonlinear least-squares regression method. The Burgers model predicted the creep responses with reasonable accuracies. A maximum of 5.83% mean absolute percentage error (MAPE) was found for the 0° infill direction and 80% infill density sample. On the contrary, the model lacks accuracy in recovery strain predictions, showing an average of 173.15% MAPE for all studied samples. Introducing Weibull's distribution improved the accuracies showing a 3.44% average MAPE for all samples.

Keywords additive manufacturing, creep and recovery, mechanical testing, tough PLA, viscoelasticity

1. Introduction

The PLA polymer is a class of aliphatic polyester that can be synthesized from renewable resources such as corn, straw and sugarcane. In addition to the polymer's synthesis attribution to agricultural sources, its biodegradability makes the polymer a promising substitute of the petroleum-based polymers in some selected applications, including fiber technology, food packaging, medical and pharmaceutical industries (Ref 1). The polymer is emerging as a sustainable material solution in biomedical engineering due to its biodegradability as well as biocompatibility (Ref 2). The PLA is used as scaffold in tissue engineering, drug delivery and encapsulation mechanisms, as well as absorbable sutures in surgeries (Ref 3). Nowadays, bioplastic developers are emerging with sustainable solutions on chemical modifications of PLA to enhance its mechanical properties. In addition, with developments in polymer blending technologies, the mechanical, rheological and thermal properties can be improved to span its application over a broader range of engineering disciplines. Although replacing petrochemical-based polymers with sustainable and bio based, or biodegradable materials is far from its full scale, promising developments are currently underway (Ref 4). Along with the development, the mechanical performances of sustainable materials are of prime importance that should be carefully studied to validate the choice of the materials in the engineering applications. In direct relevance to the applications mentioned above, understanding the viscoelastic deformation of the polymer is pivotal. In this regard, studies are made to characterize the mechanical behavior of PLA composites.

The mechanical performances of neat, glass fiber-reinforced and thermoplastic polyurethane elastomer-blended PLA composites are studied using both additive manufacturing and injection molding methods (Ref 5). Short-term mechanical tests revealed that comparable values for flexural and tensile strengths are discovered for both additive manufactured, and injection-molded specimens. The mechanical properties of additive-manufactured (FDM) and injection-molded PLA, acrylonitrile butadiene styrene (ABS) and nylon 6 polymers are studied (Ref 6). The findings suggest that the tensile strength, modulus, and elongation at break of the injection-molded samples are better than the FDM counterpart for all the cases. Correspondingly, the properties of the FDM samples from PLA are 48, 47.2 and 32.7% lower than the injection molded ones. Experimental methods are used to study the influences of printing speed and temperature (Ref 7) as well as raster angles (Ref 8) on PLA polymer. The effects of raster

Silas Z. Gebrehiwot, Department of Mechanical Engineering, Aalto University School of Engineering, Espoo, Finland; and Mechanical and Sustainable Engineering, Arcada University of Applied Sciences, Helsinki, Finland; **Leonardo Espinosa-Leal**, Graduate School and Research, Arcada University of Applied Sciences, Helsinki, Finland; **Mirja Andersson**, Mechanical and Sustainable Engineering, Arcada University of Applied Sciences, Helsinki, Finland; and and **Heikki Remes**, Department of Mechanical Engineering, Aalto University School of Engineering, Espoo, Finland. Contact e-mail: silas.gebrehiwot@arcada.fi.

Published online: 11 May 2023

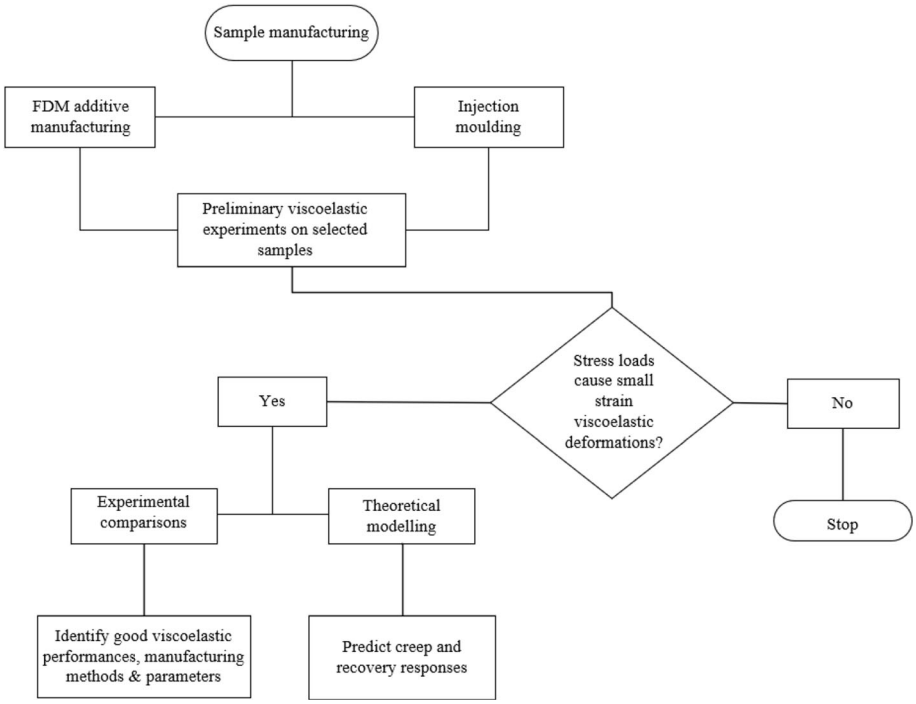

Fig.1 Flowchart demonstrating the processes followed in our methods and results

Table 1 The 3D printing parameters used to produce the tough PLA samples (Ref 26)

Printing parameters	Parameter values used
Infill orientation [°]	0°, 45°, 90°
Nozzle temperature [°C]	210
Build plate temperature [°C]	60
Orientation	Lay flat
Infill density [%]	70, 80, 90, 100%
Infill layer thickness [mm]	0.1
Infill pattern	Line
Print speed [mm/s]	50
Top/bottom layer thickness [mm]	0.5
Brim width [mm]	4
Filament diameter [mm]	2.85
Nozzle diameter [mm]	0.4

angle and moisture content on the tensile properties of additive-manufactured PLA are studied (Ref 9). An experimental method and theoretical hypothesis of transvers isotropy and classical separate-modes failure criterion are used to characterize the tensile strength at failure for additive-manufactured PLA (Ref 10). The sample variations are made based on printing angle and layer thickness. The outcomes of their experimental study indicated that the tensile strength at failure ranges between 23.56 and 54.37 MPa for increments made in printing angle and a decrement in layer thickness. The mechanical properties of graphene-reinforced PLA composite were studied using fused filament fabrication (Ref 11). The experimental study focused on characterizing the tensile and flexural strengths of the composite in relation to different build orientations. The upright printing orientation of the graphene-reinforced sample exhibited a 39.3 MPa tensile strength, and a 71.1 MPa flexural strength. Comparing to the unreinforced PLA, the strengths are 33.6 and 40.5% higher.

The influence of nanohydroxyapatite (NHA) reinforcements on the creep performance of pure PLA is studied by Feven et al. (Ref 12). The study focused on experimental investigations of the PLA nanocomposites using the dynamic mechanical analyzer (DMA). Similarly, Ans and Muammer (Ref 13) studied the creep and recovery behavior of continuous fiber-reinforced 3D-printed composites, whereas (Ref 14) investigated the creep and stress relaxation for different loading modes. The studies investigated the effects of the reinforcement fibers and temperature on the viscoelastic performances of the nanocomposites. The influence of natural fiber reinforcements on the tensile creep of the PLA polymer is studied in (Ref 15). The effect of printing parameters on the creep performances of 3D-printed PLA composite is studied in (Ref 16). The short-term tensile creep of the composite was studied experimentally by varying reinforcements and the layer thickness printing parameter. Ye et al. (Ref 17) studied the creep deformation of PLA-max material produced via fused filament fabrication. The effects of print orientation and layer thickness on the creep deformation of the polymer are studied experimentally and theoretically using a modified Burgers viscoelastic model. The four parameter Burgers model and Weibull's distribution function are used to characterize the creep and recovery of a graphene-doped rubber (Ref 18) and Polyolefin-rubber nanocomposites (Ref 19). Their findings suggest that the creep deformation and recovery strain notably depend on compositions and interfacial adhesion of constituting materials. Several literature sources reviewed the synthesis (Ref 20) the state-of-the-art in nanomedicine and biomedical applications (Ref 21, 22), mechanical properties (Ref 4) of PLA. However, most of the studies are limited to characterizing the short-term mechanical behaviors of the material in a linear elastic regime. The viscoelastic studies also focus on characterizing only the creep of the polymer with limited print parameter variants or creep and recovery of petrochemical polymers. Hence, in-depth

Table 2 The injection molding process parameters used to produce the tough PLA samples (Ref 27). The cooling time is calculated using 1D transient conduction (Ref 28)

Injection molding parameters		Set values	Note
Temperature profile, °C [23]	Feed	60	Temperature tolerances are kept at ±5 °C
	Zone 1	200	
	Zone 2	200	
	Zone 3	205	
	Nozzle	210	
Injection speed [ccm/s]		24	
Injection pressure [bar]		498—507	
Holding pressure [bar]		400—500	Linear holding profile
Melt cushion [ccm]		4.7	
Velocity/Pressure switchover [ccm]		9	Switchover is by screw position
Screw revolution [rpm]		75	
Screw back position [ccm]		34	
Cycle time [s]	Injection	1.18	The cycle time of the injection molding is 39.11*s* and includes ejection time
	Holding	10	
	Cooling	24	
	Mold open and close	2.44	
Clamping force, kN		220	

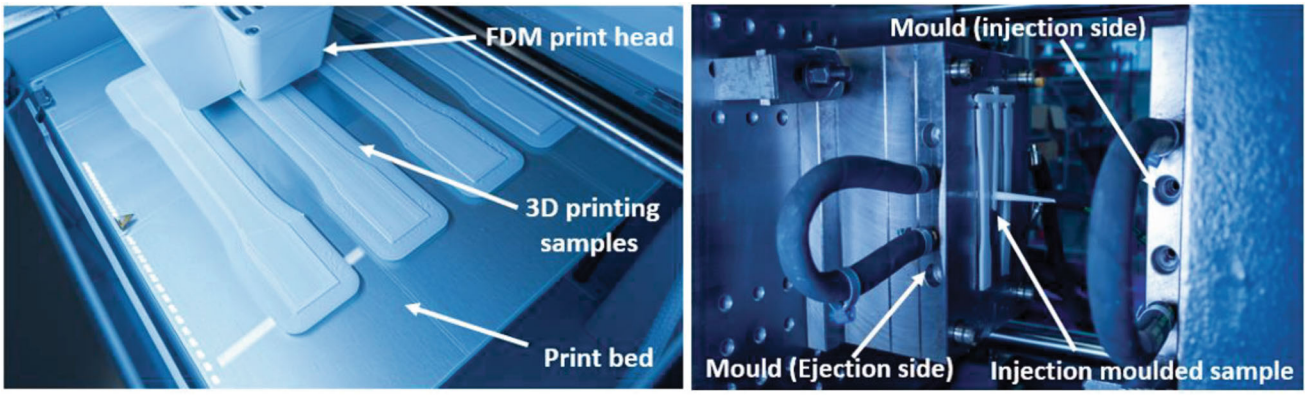

Fig. 2 Sample manufacturing processes (a) Additive manufacturing (b) Injection molding

viscoelastic creep and recovery studies of the PLA with variations in manufacturing methods, parameters and stress loadings are required to characterize the responses.

The tough PLA is currently used to manufacture functional prototypes and components used in mechanical systems. These include snap and press fits, clamps, fasteners, manufacturing aids (Ref 23, 24) and packaging containers (Ref 25). The majority of these applications induce viscoelastic deformations of the material. The objective of this paper is twofold. First, the influences of FDM process parameters on the viscoelastic deformation of the material are studied, and the results are compared to the injection-molded counterpart. For the additive manufacturing, the infill density and infill direction parameters are varied to produce 12 samples. By contrast, optimized process parameters are used to produce a single injection-molded sample variant. Second, we use the Burgers and Weibull's models to predict the creep and recovery responses of the material. The models' parameters are determined by conducting the nonlinear least-squares regression on experimental data. The accuracies of the predictions are validated using experimental data.

2. Research Methods

Our samples are designed and manufactured according to the ASTM D638 type I dimensions. The viscoelastic analyses are made on 13 sample variants produced using the additive manufacturing and injection molding methods. Our work is based on characterizing small strain viscoelastic deformations and focuses on two different goals. The first compares the viscoelastic performances of the additive-manufactured and injection-molded samples. As we have a variety of comparable sample categories, it is important to identify appropriate creep loads to visualize the samples' viscoelastic responses. The second one is on predicting the creep and recovery responses of the samples. The deformations should be within the linear

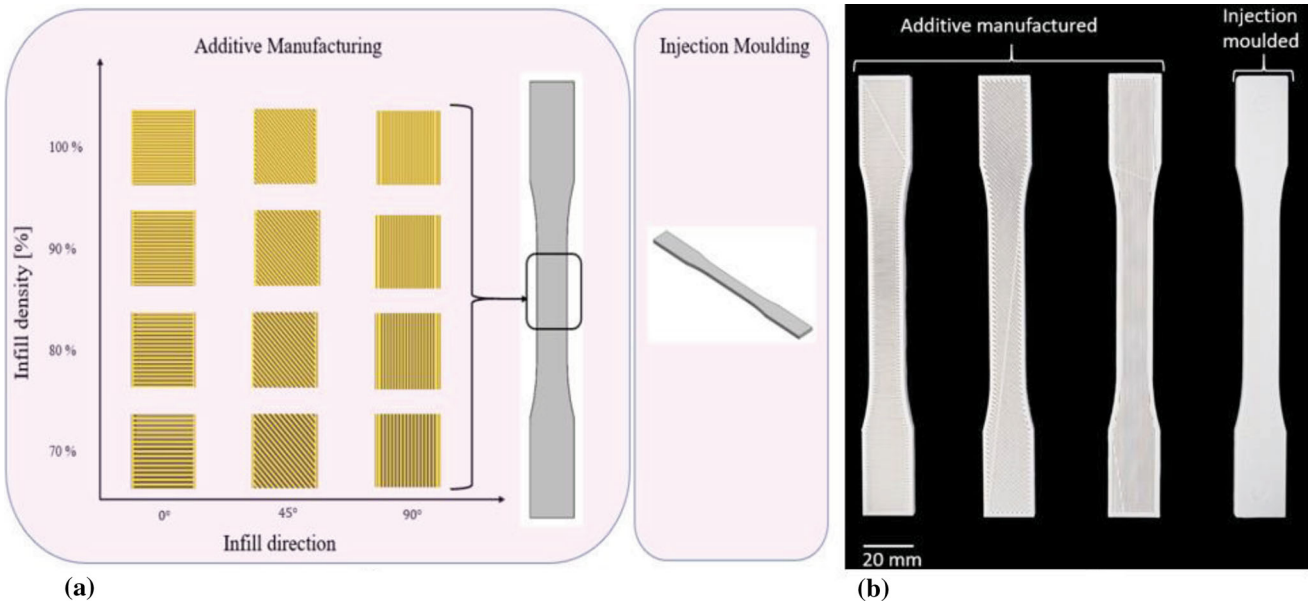

Fig. 3 Sample variants considered for the viscoelastic studies. (a) Planned (b) Manufactured using additive manufacturing and injection molding technologies

Table 3 Preliminary creep tests made at different stress loadings. The outcome of the tests differentiates the loadings which cause linear and nonlinear creep deformations

	Sample variants		Stress loadings, MPa						
Manufacturing methods	**Infill density,%**	**Infill direction, °**	σ_1	σ_2	σ_3	σ_4	σ_5	σ_6	σ_7
Additive manufactured	70	0	5	6.5	7.5	10	-	-	-
	70	45	5	6.5	7	7.5	-	-	-
	70	90	6.5	10	12.5	15	17.5	20	-
Injection molded	Injection-molded sample		6.5	10	15	17.5	20	22.5	25

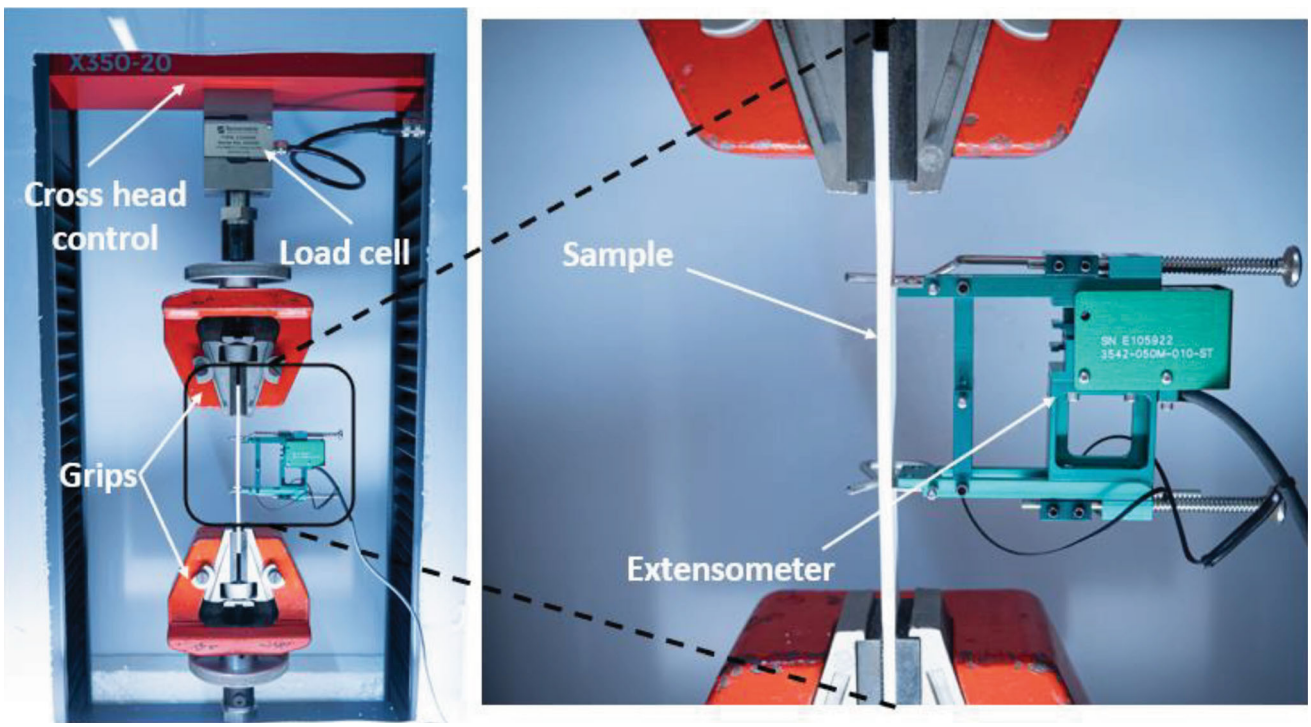

Fig. 4 Experimental setup of the viscoelastic experiments. The extensometer mounted on the samples measures the creep and recovery strain under the step tensile loadings

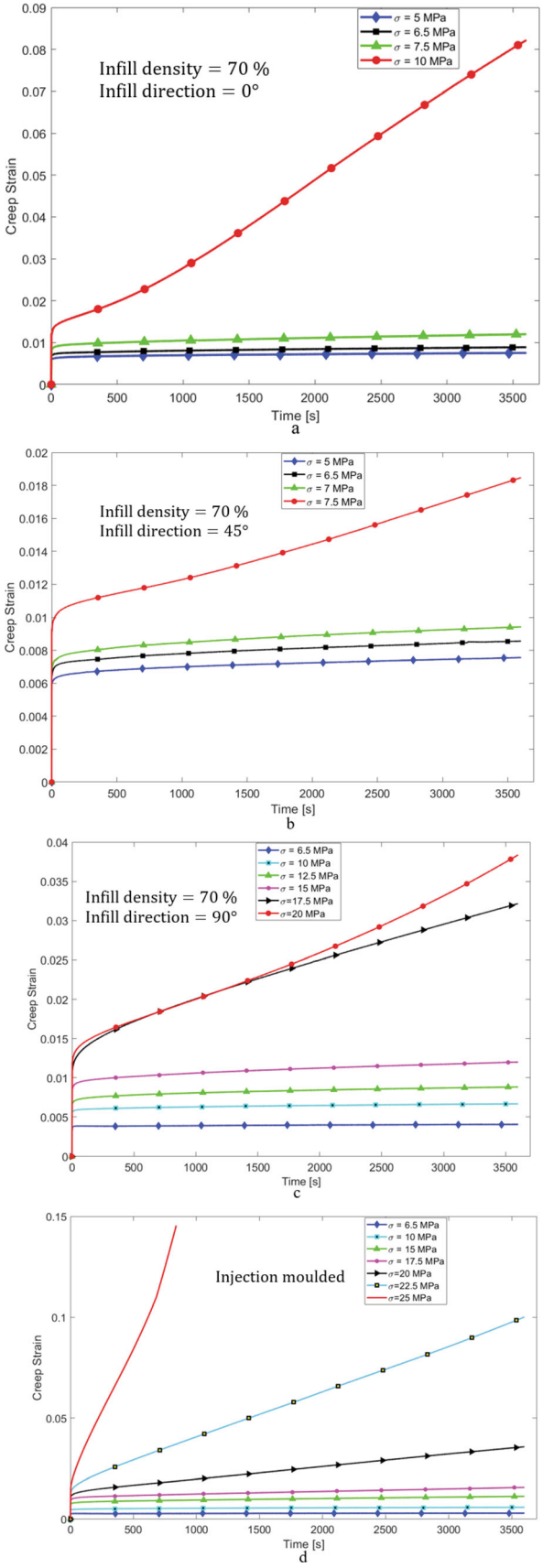

◀**Fig. 5** The creep responses of the preliminarily selected samples studied under different stress loadings. (a) Creep response of the 70% infill density and 0° infill direction. (b) Creep response of the 70% infill density and 45 ° infill direction. (c) Creep response of the 70% infill density and 90° infill direction. (d) Creep response of the injection-molded sample

viscoelastic regime to model the theoretical responses. To expedite the process of the experimental comparisons and the theoretical modeling, we follow a procedure in our methods, see Fig. 1.

2.1 Sample Manufacturing

We used FDM for additive manufacturing and a numerically controlled injection molding machine for the conventional approach.

2.1.1 Additive Manufacturing. We used the Ultimaker S3 dual extrusion fused deposition modeling (FDM) printer for additive manufacturing. The build plate was kept at 60 °C, whereas the nozzle temperature was set to 210 °C during the printing process. Appropriate pre-print adjustments including calibration, maintaining constant room temperature, cleaning the print bed were made to avoid warping and delamination. The print adhesions to build plate were secured by optimizing the brim adhesion. We produced 12 sample variants with various infill densities and infill directions. Each infill direction has four infill density variants. We used a 0.1 mm infill layer thickness and kept the top and bottom thicknesses at 0.5 mm. A line infill pattern and all other recommended parameters are used for 3D printing the sample variants. Table. 1 summarizes the printing parameters used to manufacture the samples.

2.1.2 Injection Molding. To produce the samples conventionally, we used a two-cavity mold on IntElect 50, a numerically controlled injection molding machine. At the pre-processing stage, we placed the polymer into the NOV drier for 24 h at a temperature of 55 °C to remove the moisture contained. During injection, the process parameters such as zone-temperature, nozzle temperature, screw rotation, injection speed, packing profile and clamping force were carefully optimized by continuously varying the settings. The mold temperature, T_w was kept at 45°C, whereas the nozzle temperature was 210°. The average ejection temperature, $T_e \approx$ 60°C. After each injection cycle, the samples' dimensions are measured to confirm their quality. Table 2 presents the injection molding process parameters used to manufacture samples.

The process parameters in Table 1 and 2 were followed to produce required samples using the FDM and injection molding technologies. Figure 2 shows the processing technologies used while manufacturing the samples.

Each round of additive manufacturing took close to 4.5 h (four samples at a time). By comparison, it only took 1.3 min to produce four samples using the injection molding process. Figure 3 presents the sample categories planned and produced using both technologies.

2.2 Viscoelastic Experiments

Prior to the experimental analyses and theoretical modeling, we selected a group of sample variants and tested them for creep at different stress loads. These preliminary experiments reveal the viscoelastic responses of the selected samples.

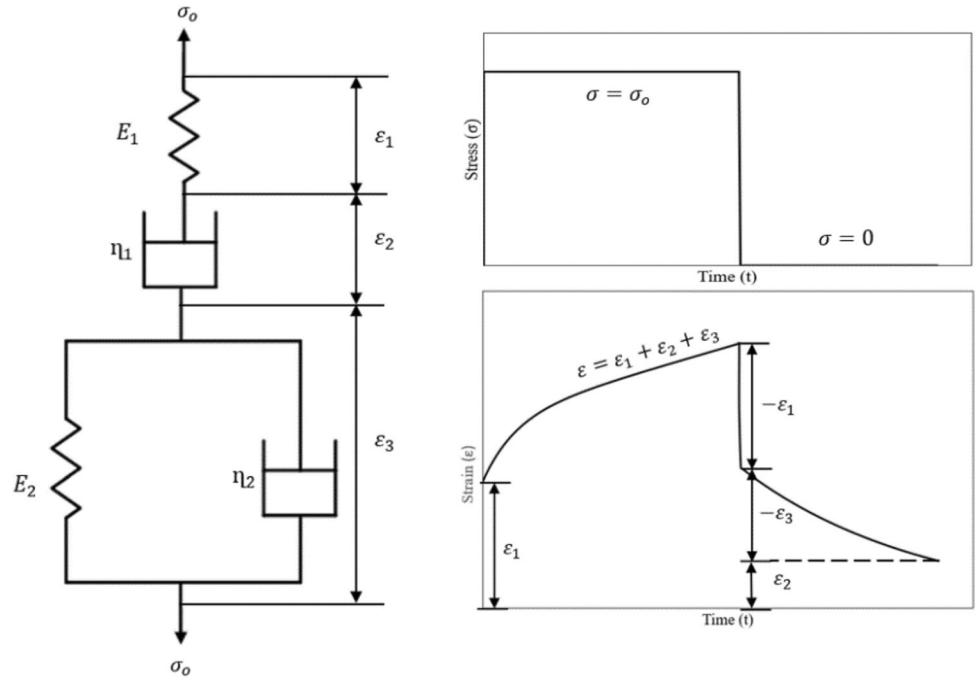

Fig. 6 The Burgers viscoelastic model and its strain response for a step tensile loading, $\sigma = \sigma_o H(t)$

Table 4 Stress loadings used during curve fitting and creep recovery predictions

	Sample		Stress loadings, MPa	
Manufacturing methods	**Infill direction, °**	**Infill density, %**	**Creep curve fitting at σ_o**	**Creep recovery prediction at σ_o**
Additive manufactured	0	70	5	7.5
		80	5	7.5
		90	8.5	9.5
		100	8.5	10
	45	70	6.5	7.5
		80	5	6
		90	7.5	8.5
		100	10	12.5
	90	70	15	16
		80	16	17.5
		90	20	17.5
		100	17.5	20
Injection molded	Injection-molded sample		15	17.5

Hence, they are used as the basis for selecting stress loads in the experimental comparisons and theoretical modeling. We selected the injection molded and the 70% infill density samples at 0°, 45°, and 90° infill directions for the preliminary tests. The choices of the samples are based on the need to identify stress loads causing linear viscoelastic deformations of the injection molded and low infill density samples. Table 3 presents the list of selected samples and the stress loadings used during the preliminary creep tests.

The viscoelastic experiments include the creep and recovery tests made using the X350-20 machine from Testometric. Each sample went through a 1 h creep followed by a 30 min recovery experiment. In the preliminary tests, the selected samples are only tested in creep. We used a step function to define the loading and unloading of the stress amplitude in the creep and recovery tests. For the viscoelastic experiments, the load sequence is defined as $\sigma = \sigma_o$ at $t = 0$ and $\sigma = -\sigma_o$ at $t = 3600$s. After unloading, the stress returns to zero, and the creep recoveries of the samples are studied for the next 1800 s. The frequency of data recording under the step tensile stress functions is set at 150Hz. This generated more than half a million strain–time data for each test. The data are recorded using Epsilon technology's high-precision digital extensometer TE3442. Figure 4 shows the experimental setup where a sample is attached to the clip-on extensometer and clamped in the wedge grips.

The outcomes of the preliminary creep tests under different stress loadings show the different viscoelastic responses of the samples. The samples' creep responses depend on the stress loadings used during the step tensile tests.

The creep responses of the samples in Fig. 5(a-d) indicate the linear and nonlinear viscoelastic responses of the material. The creep of a material is classified into three stages; primary, secondary, and tertiary (Ref 29). The primary stage includes the

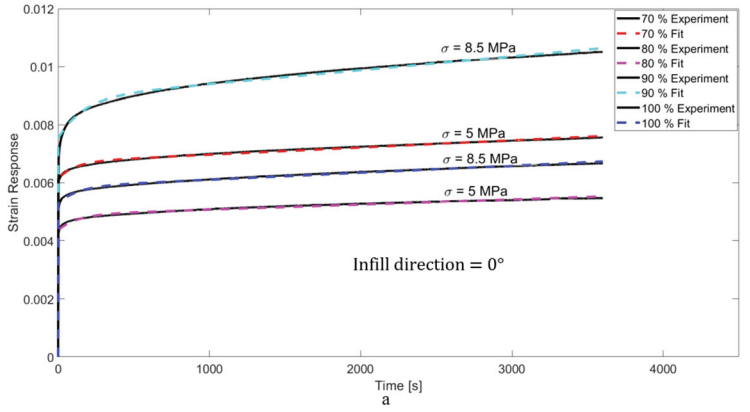

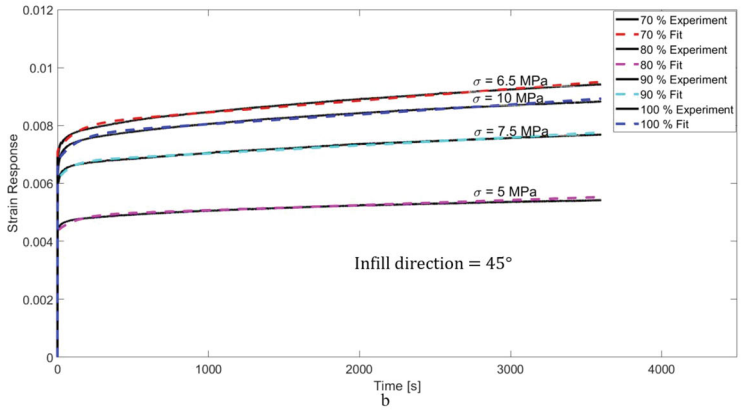

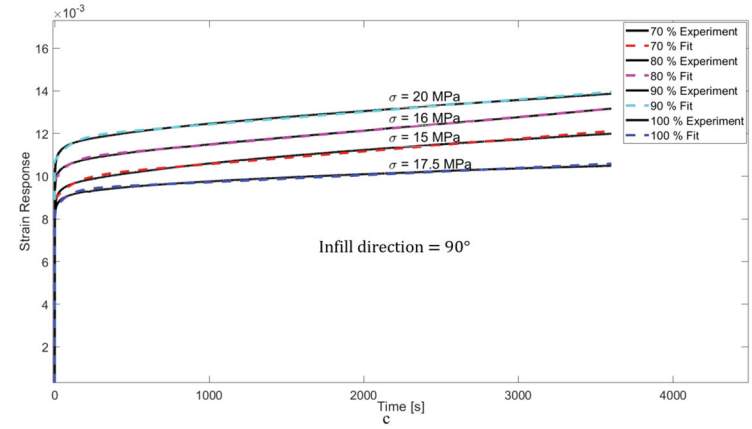

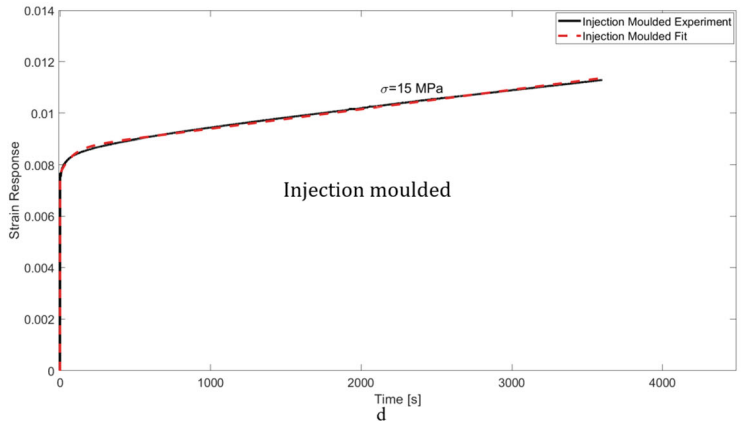

Fig. 7 Curve fitting of the Burger viscoelastic model to experimental creep. (a) Additive-manufactured samples with 0° infill direction. (b) Additive-manufactured samples with 45° infill direction. (c) Additive-manufactured samples with 90° infill direction. (d) Injection-molded sample

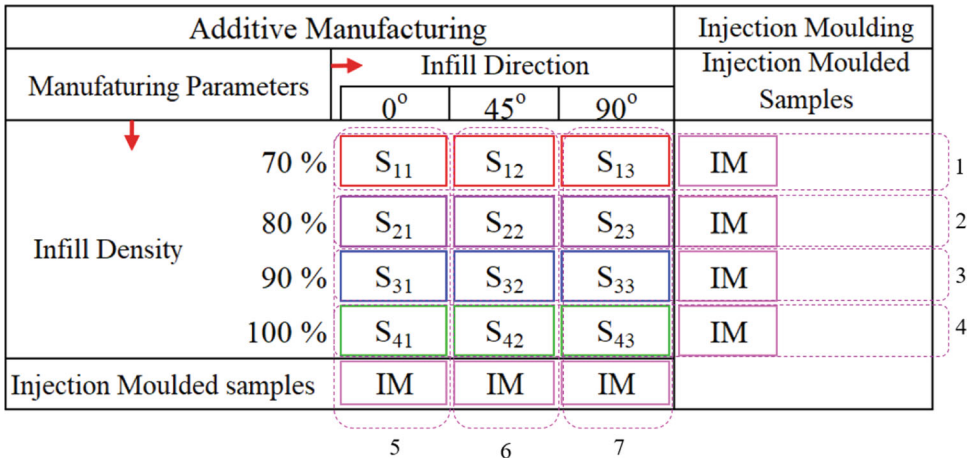

Fig. 8 Comparisons of experimentally studied samples categorized based on the manufacturing methods. The additive-manufactured sample variants are presented using matrix notations representing the combined infill density and infill direction information. The injection-molded sample has a single sample variant with IM abbreviations in each cell

instantaneous deformation and the time dependent strain, which occurs at a decreasing rate. The secondary stage is also known as a steady state, where the strain rate becomes nearly constant. It characterizes the viscous flow of the material. The tertiary stage occurs with an increased strain rate and leads to a complete viscoelastic rupture (Ref 29). The linear viscoelasticity models are applicable in small strain deformations that occur majorly at the primary stage of a creep (Ref 30). With an increase in stress loadings, the secondary and tertiary stages of the creep dominate materials' viscoelastic deformations. The secondary creep stage of materials is characterized using empirical power functions, such as the one developed by Findely, Khosla and Peterson, which adequately predicted the nonlinear viscoelastic deformation (Ref 29, 31).

In Fig. 5(a), the 70% infill density and 0° infill direction sample showed a linear viscoelastic deformation up to 7.5MPa. However, when stress loading is increased to 10MPa, a dominant secondary stage creep with a sharp increment in the viscoelastic deformation is observed. Similarly, a 7.5MPa loading caused, a nonlinear viscoelastic deformation for the 70% infill density and 45 ° infill direction sample, see Fig. 5(b). In Fig. 5(c), we observed the linear viscoelastic responses of the 70% infill density and 90° infill direction sample when the load increments were made up to 15MPa. Secondary and tertiary creep phenomena were observed at 17.5 and 20MPa loadings, respectively. For the injection-molded sample presented in Fig. 5(d), the responses remained in the linear viscoelastic regime for the stress loadings up to 15MPa. However, the sample showed a secondary stage creep behavior for the 17.5, 20 and 22.5 MPa loadings. Even if the deformations remained at the secondary stage, the increase in stress exasperated the creep responses. With a further increment in stress to 25 MPa, we observed a swift transition of the creep to the tertiary stage within the first 650s. Figure 5 (a)-(d) shows the different stages of the creep responses for the selected samples. They are the basis for the subsequent experimental and theoretical analyses.

2.3 Theoretical Characterizations of Creep and Recovery

Linear viscoelasticity refers to materials' time-dependent strain (response) for a stress input. It characterizes the viscous and elastic responses of materials, mainly polymers. The viscous behavior is represented by dashpot constants (η_i), whereas the elastic one is characterized using spring constants (E_i) (Ref 32). Under infinitesimal strain and strain rate conditions, the time-dependent stress–strain relations are presented using linear differential equations (Ref 33). The differential form of the constitutive equation for viscoelastic materials is (Ref 34)

$$\sum_{i=0}^{n} p_i \frac{\partial^i \sigma}{\partial t^i} - \sum_{i=0}^{m} q_i \frac{\partial^i \varepsilon}{\partial t^i} = 0. \quad \text{(Eq 1)}$$

In Eq 1, i indicate the order of differential, p_i and q_i represent the various combinations of the rheological constants of the material, whereas m and n show the number of these combinations.

2.3.1 The Burgers Model. The Burgers model is a four-parameter viscoelastic model which has a single Maxwell connected in series with a Kelvin–Voigt. The constitutive of the Burgers model can be derived from Eq 1 as (Ref 33)

$$p_0\sigma + p_1\dot{\sigma} + p_2\ddot{\sigma} = q_1\dot{\varepsilon} + q_2\ddot{\varepsilon}. \quad \text{(Eq 2)}$$

The stress loading in tensile creep, σ is usually defined by a step function (Ref 32),

$$\sigma = \sigma_o H(t). \quad \text{(Eq 3)}$$

In Eq 3, $H(t)$ is a Heaviside step function that defines the stress as $\sigma_{t\to 0^-} = 0$, and $\sigma_{t\to 0^+} = \sigma_o$ (Ref 34). The creep of the Burgers model is the sum of the individual strain responses of the rheological models connected in series, see Fig. 6. The first spring, E_1 undergoes instantaneous deformation when, $\sigma_{t\to 0^+} = \sigma_o$. As time increases, the first dashpot, η_1 deforms linearly and is characterized as a non-reversible viscous flow. Together, these rheological constants represent the Maxwell branch. The strain response of the Kelvin–Voigt branch is also time dependent and is referred to as delayed elasticity.

The creep of the Burgers model in Fig. 1 is (Ref 34)

$$\varepsilon(t) = \varepsilon_1 + \varepsilon_2 + \varepsilon_3. \quad \text{(Eq 4)}$$

The strains in Eq 4 are further given as functions of the material's rheological constants and the applied stress (Ref 29). That is

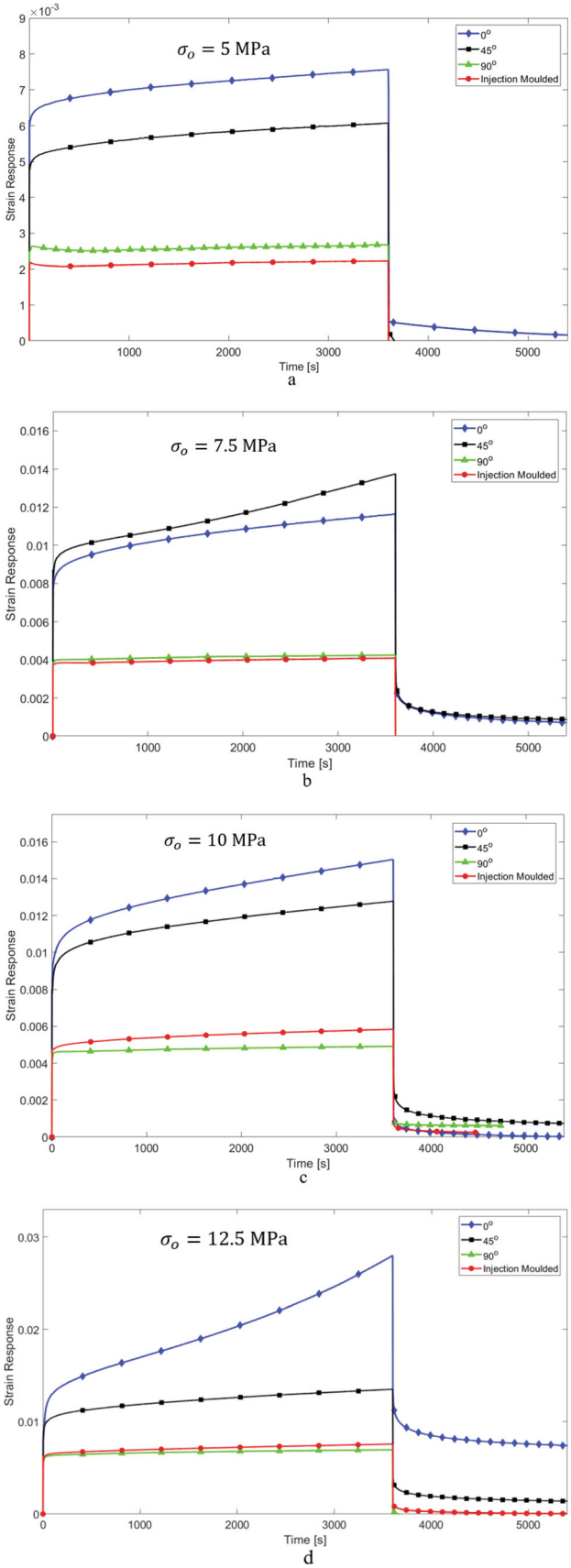

◀**Fig. 9** Creep and recovery responses of the injection-molded and additive-manufactured samples. The different infill directions are studied in each category. (a) Creep and recovery of the IM and 70% infill density samples at $\sigma_o = 5$MPa. (b) Creep and recovery of the IM and 80% infill density samples at $\sigma_o = 7.5$MPa. (c) Creep and recovery of the IM and 90% infill density samples at $\sigma_o = 10$MPa. (d) Creep and recovery of the IM and 100% infill density samples at $\sigma_o = 12.5$MPa

$$\varepsilon_1 = \frac{\sigma}{E_1}, \dot{\varepsilon}_2 = \frac{\sigma}{\eta_1}, \dot{\varepsilon}_3 + \frac{E_2}{\eta_2}\varepsilon_3 = \frac{\sigma}{\eta_2}. \quad \text{(Eq 5)}$$

The constitutive equation of the model can be derived by taking the Laplace transform of strains in Eq 5. The stress and strain relations in the Laplace domain can be derived from Eq 4 and 5 as (Ref 34)

$$\overline{\varepsilon}(s) = \frac{\tilde{\sigma}(s)}{E_1} + \frac{\tilde{\sigma}(s)}{s\eta_1} + \frac{\tilde{\sigma}(s)}{\eta_2\left(s + \frac{E_2}{\eta_2}\right)}. \quad \text{(Eq 6)}$$

The inverse of the Laplace transform for Eq 6 gives the constitutive of the viscoelastic model with determined coefficients (Ref 32).

$$\frac{\eta_1\eta_2}{E_2}\ddot{\varepsilon} + \eta_1\dot{\varepsilon} = \frac{\eta_1\eta_2}{E_1E_2}\ddot{\sigma} + \left(\frac{\eta_1}{E_1} + \frac{\eta_2}{E_2} + \frac{\eta_1}{E_2}\right)\dot{\sigma} + \sigma. \quad \text{(Eq 7)}$$

Using the initial conditions and boundary load information, Eq 7 can be solved to determine the creep of the Burgers model as (Ref 29)

$$\varepsilon(t) = \sigma_0\left[\frac{1}{E_1} + \frac{1}{\eta_1}t + \frac{1}{E_2}\left(1 - e^{-\frac{E_2}{\eta_2}t}\right)\right]. \quad \text{(Eq 8)}$$

In Eq 8, the expression on the right shows the instantaneous elasticity, permanent deformation and delayed elasticity terms, respectively. The creep of the model presented in Eq 8 is for a constant stress input. However, the step loading can be intermittent, which influences the creep response of the model (Ref 35). Under this condition, the resulting strain can be evaluated using the Boltzmann superposition principle, where the strain responses of the individual stress loading are superimposed (Ref 36). The strain response of a viscoelastic material under a varying step stress loading is (Ref 35)

$$\varepsilon(t) = \sum_{i=1}^{n} \Delta\sigma_i * J(t - t_i). \quad \text{(Eq 9)}$$

In Eq. (9), $\Delta\sigma_i$ are the step changes made in stress at the corresponding times, t_i. $J(t - t_i)$ represents the creep compliance of the material at each load transition. From Eqs 8 and 9, the creep compliance of the Burgers model can be defined as (Ref 35)

$$J(t - t_i) = \left[\frac{1}{E_1} + \frac{1}{\eta_1}(t - t_i) + \frac{1}{E_2}\left(1 - e^{-\frac{E_2}{\eta_2}(t - t_i)}\right)\right]. \quad \text{(Eq 10)}$$

When a viscoelastic material is initially loaded with a constant stress σ_0, the material undergoes a creep deformation. If the load is fully removed after some time, the material gradually recovers part of the creep deformation. The Burgers

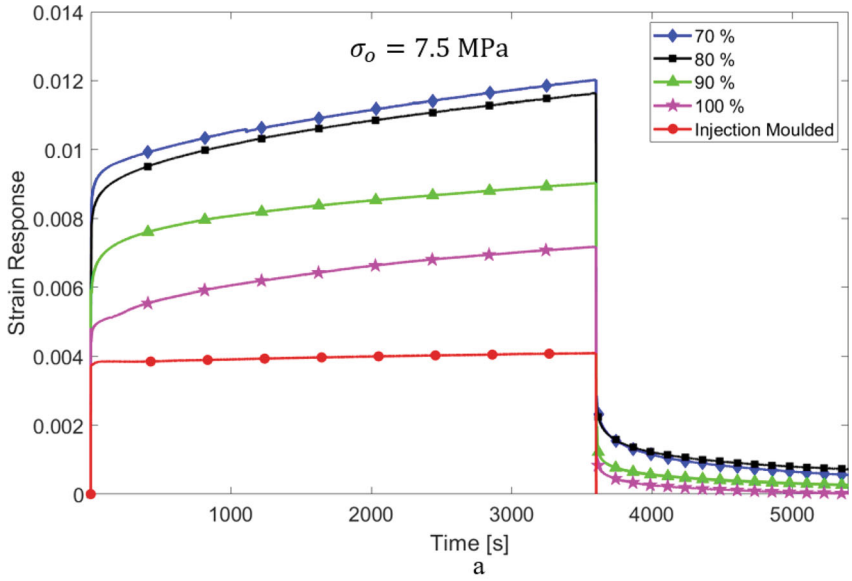
σ_o = 7.5 MPa
70 %
80 %
90 %
100 %
Injection Moulded
Strain Response
Time [s]
0.014
0.012
0.01
0.008
0.006
0.004
0.002
0
1000
2000
3000
4000
5000

a

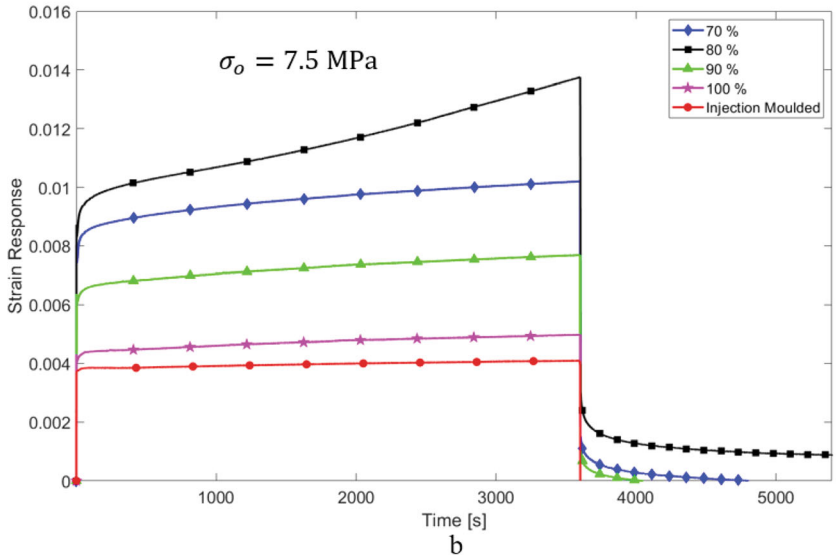
σ_o = 7.5 MPa
70 %
80 %
90 %
100 %
Injection Moulded
Strain Response
Time [s]
0.016
0.014
0.012
0.01
0.008
0.006
0.004
0.002
0
1000
2000
3000
4000
5000

b

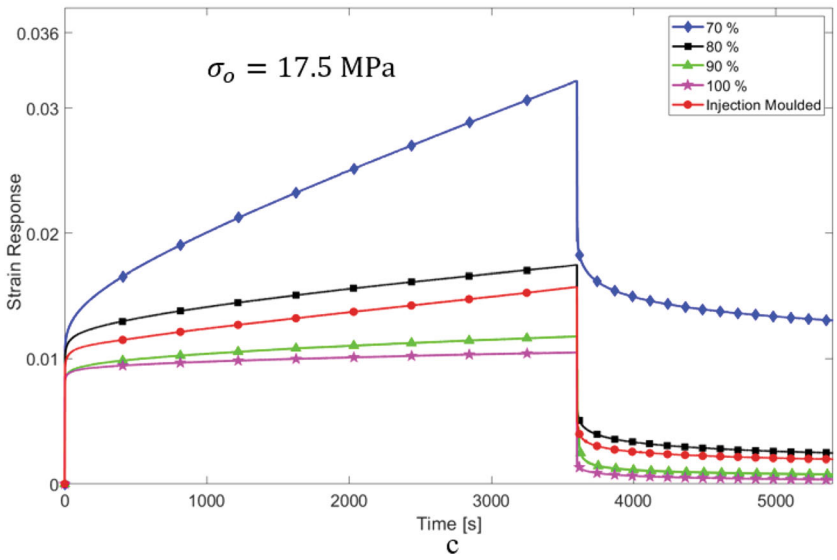
σ_o = 17.5 MPa
70 %
80 %
90 %
100 %
Injection Moulded
Strain Response
Time [s]
0.036
0.03
0.02
0.01
0
0
1000
2000
3000
4000
5000

c

◀**Fig. 10** Experimental creep and recovery responses of the injection-molded and additive-manufactured samples. The different infill densities are studied in each category for the additive-manufactured samples. (a) Creep and recovery of the IM and 0° infill direction samples at $\sigma_o = 7.5$MPa. (b) Creep and recovery of the IM and 45° infill direction samples at $\sigma_o = 7.5$MPa. (c) Creep and recovery of the IM and 90° infill direction samples at $\sigma_o = 17.5$MPa

model makes use of Eqs 9 and 10 to predict the creep recovery of the material as (Ref 33)

$$\varepsilon(t) = \sigma_o \left[\frac{1}{\eta_1}(t_2 - t_1) + \frac{1}{E_2}\left(e^{-\frac{E_2}{\eta_2}(t-t_2)} - e^{-\frac{E_2}{\eta_2}(t-t_1)} \right) \right]. \quad \text{(Eq 11)}$$

In Eq 11, t_1 and t_2 represent the times when the step stress is loaded and unloaded, respectively.

2.3.2 Weibull's Distribution. The accuracies of the viscoelastic modeling using springs and dashpots depend on the number of elements used to predict the viscoelastic responses, which occur on wide distributions of relaxation or retardation times (Ref 37). Often, the use of generalized models with several spring-dashpot elements improves the accuracy; however, it comes with mathematical complexities (Ref 38). The viscoelastic recovery of polymeric materials can be accurately modeled using the Weibull's distribution function. The approach uses time-dependent latches to model the viscoelastic recovery as distributions of the latch trigger times (Ref 38). The time-dependent recovery strain, $\varepsilon_r(t)$ over the recovery time, t is given as (Ref 38)

$$\varepsilon_r(t) = \varepsilon_v \left[e^{-\left(\frac{t}{\eta_r}\right)^{\beta_r}} \right] + \varepsilon_f. \quad \text{(Eq 12)}$$

In Eq 12, ε_v is a function for the viscoelastic recovery of the material that is determined by the Weibull shape parameter, β_r and the characteristic life, η_r. The ε_f is the permanent viscoelastic deformation due to the viscous flow.

2.4 Curve Fitting

Based on the outcomes of preliminary viscoelastic tests, we selected the stress loads for linear viscoelastic modeling. The regression analyses are first made using the nonlinear least-squares method to predict the samples' responses theoretically. The creep and recovery sections of the data are separately fit to the Burgers and Weibull's equations to determine the models' parameters shown in Eq 8 and 12. The curve fittings are made using MATLAB numerical software. For each sample, the rheological constants that are determined at one stress loading will be used to predict the creep and recovery responses at another stress loading. Table 4 presents the list of all stress loadings used for the curve fitting and viscoelastic response predictions.

We used the Levenberg–Marquardt algorithm and monitored the robustness of the nonlinear least-squares fitting by adjusting starting points of the coefficients (rheological constants). Within the 95% confidence bounds the adjusted R-Squares of all the fits are greater than 0.96. Figure 7(a)-(d) shows the creep curve fitting for the sample variants presented in Table. 4.

3. Results and Discussion

We present the results of the experimental and theoretical viscoelastic studies in this chapter. The experimental findings focus on comparisons of the samples' viscoelastic responses. The samples are first manufactured using the FDM additive manufacturing and injection molding methods. Then, creep and recovery experiments are made using different stress loadings. The experimental creep and recovery results of 13 different sample variants (12 additive manufactured and 1 injection molded) are studied and compared. The theoretical studies focus on predicting the viscoelastic responses of the samples using the Burgers and Weibull's models. The creep responses of the samples are used to determine the Burgers viscoelastic parameters via the nonlinear least-squares curve fitting. The determined parameters are used to predict the creep and recovery responses at new stress loadings. The Weibull's

Table 5 Rheological constants of the Burgers viscoelastic model determined by regression

	Samples		Rheological constants			
			Elastic constants, GPa		Dashpot constants, GPa s	
Manufacturing methods	Infill direction, °	Infill density, %	E_1	E_2	η_1	η_2
Additive manufactured	0	70	0.82	8.64	15100	947
		80	0.95	9.08	10900	1160
		90	1.01	4.52	11200	1000
		100	1.53	12.2	25200	1880
	45	70	1.01	7.06	17000	663
		80	1.01	9.38	28500	1160
		90	1.12	11.2	24500	1030
		100	1.31	9.17	21000	1140
	90	70	1.58	11.1	16100	1720
		80	1.59	10.1	15500	1370
		90	1.99	19.9	36,000	1800
		100	2.01	10.8	30800	1560
Injection molded	Injection-molded sample		1.79	15.1	14500	1190

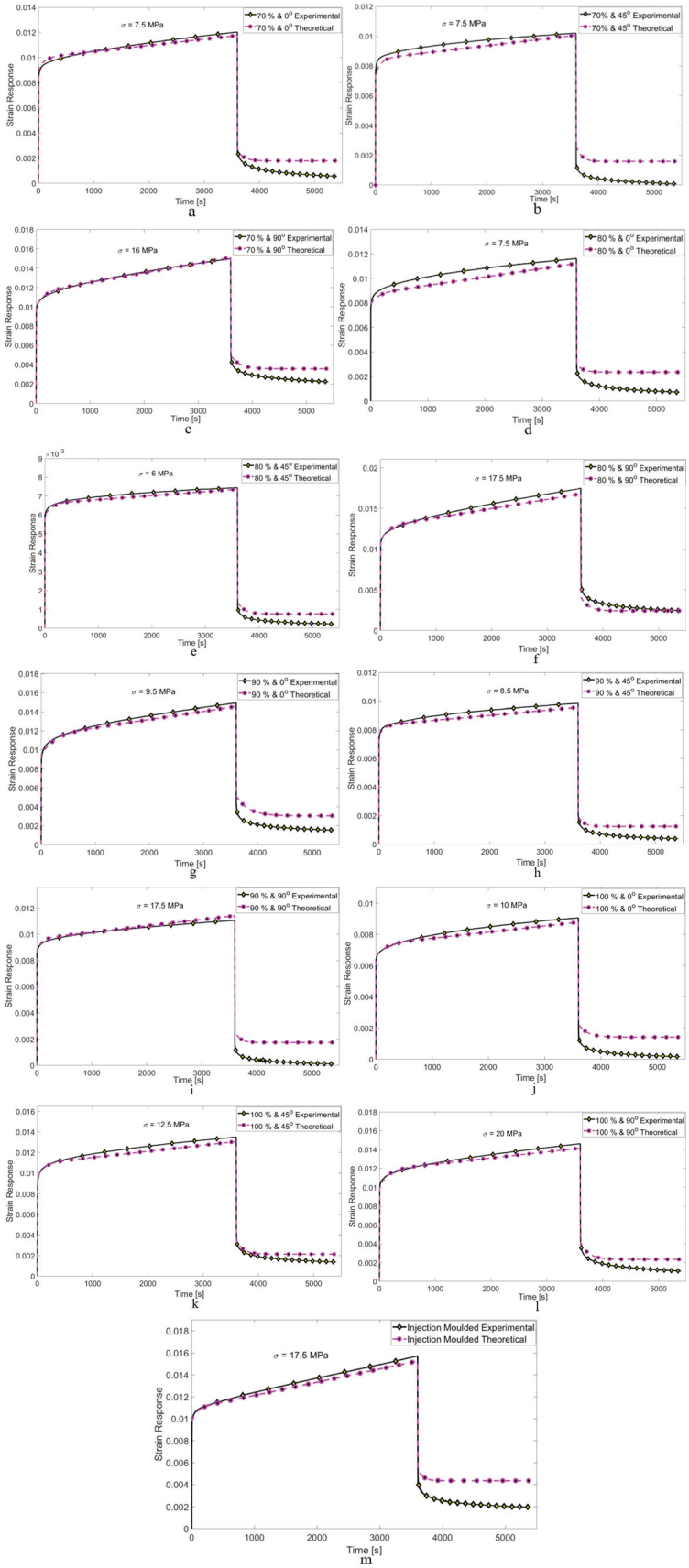
σ = 7.5 MPa
70 % & 0° Experimental
70 % & 0° Theoretical
Strain Response
Time [s]
a
σ = 7.5 MPa
70% & 45° Experimental
70% & 45° Theoretical
Strain Response
Time [s]
b
σ = 16 MPa
70 % & 90° Experimental
70 % & 90° Theoretical
Strain Response
Time [s]
c
σ = 7.5 MPa
80 % & 0° Experimental
80 % & 0° Theoretical
Strain Response
Time [s]
d
σ = 6 MPa
80 % & 45° Experimental
80 % & 45° Theoretical
Strain Response
Time [s]
e
σ = 17.5 MPa
80 % & 90° Experimental
80 % & 90° Theoretical
Strain Response
Time [s]
f
σ = 9.5 MPa
90 % & 0° Experimental
90 % & 0° Theoretical
Strain Response
Time [s]
g
σ = 8.5 MPa
90 % & 45° Experimental
90 % & 45° Theoretical
Strain Response
Time [s]
h
σ = 17.5 MPa
90 % & 90° Experimental
90 % & 90° Theoretical
Strain Response
Time [s]
i
σ = 10 MPa
100 % & 0° Experimental
100 % & 0° Theoretical
Strain Response
Time [s]
j
σ = 12.5 MPa
100 % & 45° Experimental
100 % & 45° Theoretical
Strain Response
Time [s]
k
σ = 20 MPa
100 % & 90° Experimental
100 % & 90° Theoretical
Strain Response
Time [s]
l
σ = 17.5 MPa
Injection Moulded Experimental
Injection Moulded Theoretical
Strain Response
Time [s]
m

◀**Fig. 11** The theoretical creep and recovery response predictions using the Burgers viscoelastic model are presented compared to the experimental findings. (a) 70% infill density and 0° infill direction, (b) 70% infill density and 45° infill direction, (c) 70% infill density and 90° infill direction, (d), 80% infill density and 0° infill direction, (e) 80% infill density and 45° infill direction, (f) 80% infill density and 90° infill direction, (g) 90% infill density and 0° infill direction (h) 90% infill density and 45° infill direction, (i) 90% infill density and 90° infill direction, (j) 100% infill density and 0° infill direction, (k) 100% infill density and 45° infill direction, (l) 100% infill density and 90° infill direction, (m) Injection-molded samples

distribution function is introduced as an effective approach to predict the recoveries of the samples.

3.1 Experimental Findings

We observed wide variations on the strain responses of the injection molded, and additive-manufactured samples. A stress loading that causes a linear viscoelastic deformation for the injection molded and 90° infill direction samples could result in a nonlinear deformation for the 45° and 0° infill direction samples. Hence, the viscoelastic response comparisons are made separately based on the infill directions and infill densities that also include the comparable responses of the injection-

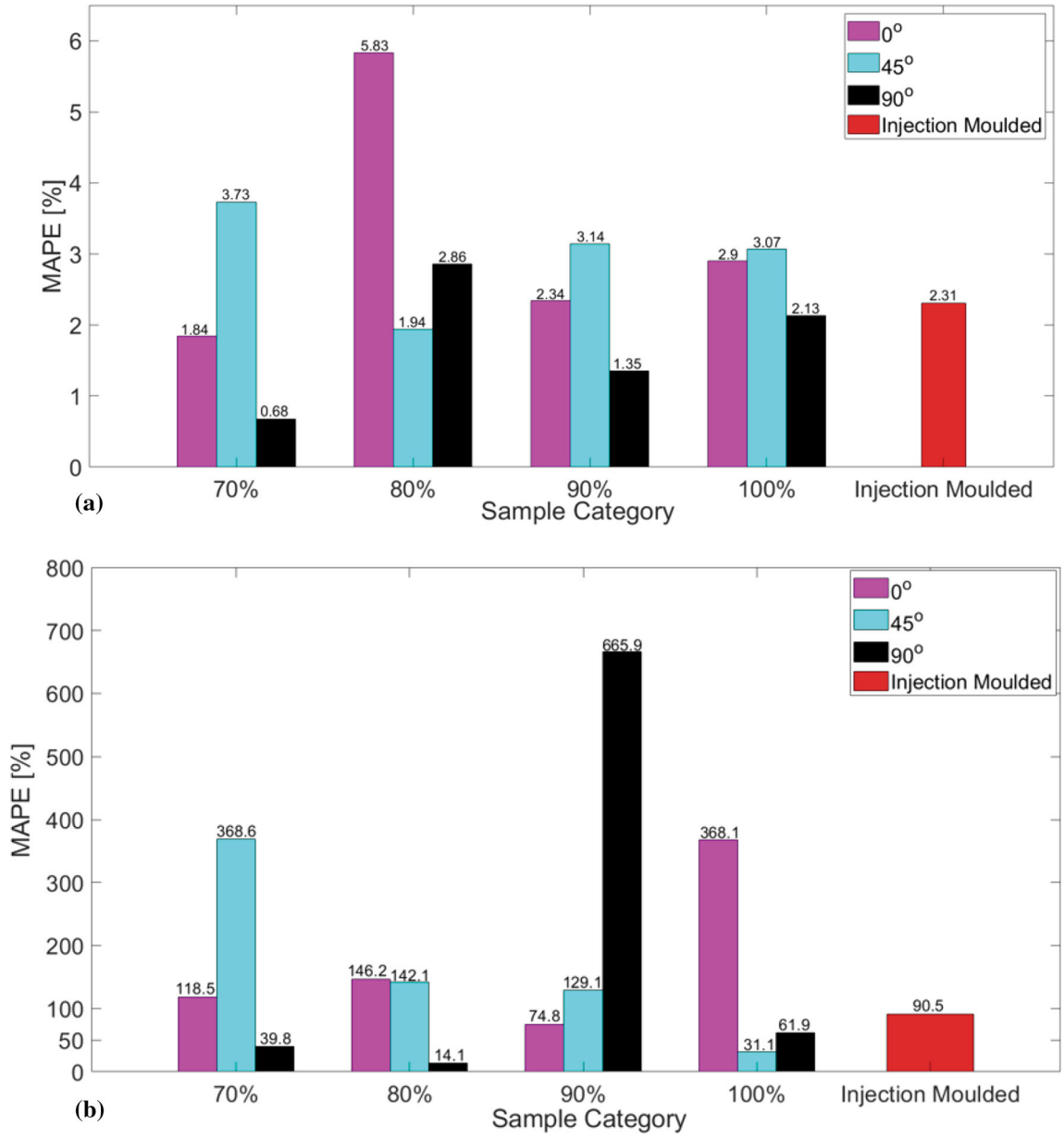

Fig. 12 The mean absolute percentage errors (MAPEs) of the Burgers viscoelastic model for (a) creep predictions (b) recovery predictions of the additive-manufactured and injection-molded samples

Table 6 The Weibull's recovery parameters of the additive-manufactured and injection-molded samples, determined using the nonlinear least-squares curve fitting

	Sample		Creep loading			Recovery parameters of Weibull's model	
Manufacturing methods	Infill Direction, °	Infill Density, %	σ	ε_v	η_r, s	β_r	ε_f
Additive manufactured	0	70	7.5	0.003426	272.1	0.3199	$2.277e^{-5}$
		80	5	0.004014	157.5	0.2323	$4.192e^{-5}$
		90	9.5	0.005910	323.1	1859	3.341e-^{5}
		100	10	0.003043	23.98	0.2464	$4.353e^{-5}$
	45	70	7.5	0.00152	225.8	0.4818	1.276^{-5}
		80	6	0.001899	64.28	0.2428	$1.714e^{-5}$
		90	8.5	0.002649	104.9	0.2749	$9.356e^{-5}$
		100	12.5	0.004906	489.1	0.2007	$3.937e^{-5}$
	90	70	16	0.004038	74.71	0.2338	$1.531e^{-4}$
		80	17.5	0.006964	1361	0.2505	$4.009e^{-5}$
		90	17.5	0.002552	37.76	0.2816	$4.424e^{-6}$
		100	20	0.005348	105.1	0.2983	$5.249e^{-5}$
Injection molded		Injection-molded sample	17.5	0.006002	543.3	0.2046	$2.318e^{-4}$

molded samples. The categories of comparison are presented with a schematic matrix in Fig. 8. The additive-manufactured sample variations are represented using a matrix notation, S_{ij}. The index i represents the infill density, whereas the j represents the infill direction variants. The injection-molded sample is a single variant represented by IM (Injection Molded) initials. Based on these, there are seven different comparisons, of which four are based on the infill direction, and the remaining three are based on infill density, see the rows and columns numbering in Fig. 8. The injection-molded sample is included in all comparison categories.

3.1.1 Infill Direction. The injection-molded and additive-manufactured samples' creep and recovery responses are experimentally studied. Figure 9(a)-(d) shows the results of the injection molded and, the additive-manufactured samples with different infill densities 70-100%. The comparisons in each subfigure are made based on infill directions.

The 0° and 45° samples generally showed the least viscoelastic performances in all comparisons. Regardless of their infill densities, both samples showed higher creep deformations compared to the 90° and the injection molded ones. At $t = 3600$s, the creep strains of the 0° samples are $2.72 - 4.03$ times higher than the 90° and $2.68 - 7.78$ times higher than the injection-molded samples. In contrast, the creep of the 45° samples is 1.95-3.24 times higher than the 90°, and $2.4 - 6.25$ times higher than the injection molded ones. In particular, the 80% and 45° sample at $\sigma_o = 7.5$MPa, as well as the 100% and 0° sample at $\sigma_o = 12.5$MPa exhibited the highest viscoelastic deformations. By comparison, their creep recoveries are also slow, see Fig. 9(b) and (d). These poor viscoelastic performances are attributed to deviations of the infill directions from the loading orientation (90°). In addition, process-related micro and mesostructure flaws contribute to higher creep deformations. On the other hand, the 90° FDM samples show excellent viscoelastic performances. The elastic behavior of these samples dominates the viscous flow at all stress loadings. The smaller viscoelastic deformations are due to the infill reinforcements in the loading direction (90°). The injection-molded samples showed smaller creep deformations at lower stresses, such as 5 and 7.5MPa. Their viscoelastic performances are also good at higher stresses; however, slightly lower than the 90° samples.

3.1.2 Infill Density. The influence of the infill density on the creep and recovery responses of the additive-manufactured samples is studied and compared to the injection molded ones, see Fig. 10(a)-(c). For the additive-manufactured samples, the study is categorized based on the 0°, 45° and 90° infill directions.

The additive-manufactured samples showed a decreasing creep deformation with the increase in infill density. This behavior holds for all infill directions except for the 45° with 80% infill density sample in Fig. 10(b). The increase in infill density is expected to decrease the volumes of the interlayer voids which creates stronger adhesions between adjacent layers. On the other hand, injection-molded samples exhibited a predominantly linear elastic deformation at lower stress loadings. Comparing the viscoelastic creep and recovery, injection-molded samples are better than all infill density samples in the 0° and 45° infill direction categories, see Fig. 10 (a) and (b). The 80% infill density sample with 45° infill direction showed the poorest viscoelastic response, exhibiting higher creep deformation at 7.5MPa loading. Most of the 90° infill direction samples showed excellent viscoelastic performances, which are comparable and, in some cases, superior to the responses of the injection molded ones. At $t = 3600$ s, the creep strains of the 90 and 100% infill density samples in Fig. 10(c) are 25.17 and 36.14% less than the injection molded ones. On the other hand, the 70% infill density sample showed a higher creep leading to a viscous flow at 17.5MPa loading (see Fig. 10c).

3.2 Creep and Recovery Prediction Using the Burgers Model

We determined the Burgers rheological constants via the regression analyses in the previous chapter. These constants are determined for each sample variant considered in the fitting process, see Table 4 and Fig. 7(a-d). We observed certain

similarities among the values of comparable rheological constants determined for the samples, see Table 5. The determined spring and dashpot constants are used to predict the creep and recovery responses of the samples at new stress loadings. We used Eq 8 and 11 to estimate the theoretical creep and recovery responses, respectively. The creep and recovery prediction of the 13 different samples with variations on the method of manufacturing and print parameters are presented, see Table 4 and 5, and Fig. 11(a)-(m).

The Burgers viscoelastic model shows that the creep and instantaneous recovery predictions are in good agreement with the experimental results. However, in most cases, the long-term recoveries are not well predicted by the model, see Fig. 11 (a-m). In order to validate the theoretical approach, the prediction errors in creep and recovery are separately evaluated. The mean absolute percentage error (MAPE), a typical method for evaluating accuracies of predictive models (Ref 40) is used for the analyses. For N data points, the MAPE is given as (Ref 39)

$$\mathrm{MAPE} = \frac{1}{\mathrm{N}}\sum_{\mathrm{t}=1}^{\mathrm{N}}\left|\frac{\varepsilon - \varepsilon_{\mathrm{B}}}{\varepsilon}\right| * 100\%. \qquad \text{(Eq 13)}$$

In Eq 13, ε is the experimental strain, and ε_B is the strain predicted using the Burgers model. The MAPE of the Burgers model in creep and recovery predictions are evaluated and presented in Fig. 12(a) and (b).

Based on the analyses in Fig. 12(a) and (b), there are considerable differences on the margins of error for the creep and recovery predictions. The MAPEs for the creep predictions are all minimal and exist within a tolerable margin. For the creep, a maximum of 5.83% MAPE is observed for the 0° infill direction and 80% infill density sample. In comparison, the 90° infill direction and 70% infill density sample showed a minimum of 0.68% MAPE. The injection-molded sample showed a 2.31% deviation which is less than the mean value of 2.65% for all additive manufactured ones. The error analyses in the creep sections showed that the calculated responses using the Burgers model are in good agreement with experimental results. On the contrary, the recovery responses predicted using the theoretical model showed significant deviations from the experimental findings.

The Burgers model generally lacks accuracy in predicting the recovery strains of the samples, see Fig. 12(b). The theoretical recovery predictions are calculated using Eq 11, which contains a permanent deformation of the first dashpot (ε_2) and the recovery of delayed elasticity from the Kelvin–Voigt branch ($-\varepsilon_3$), see Fig. 1. In the theoretical analyses, the permanent deformations of the dashpot (η_1), are overestimated. In addition, the recoveries of the delayed elasticity are slow in the theoretical model, see Fig. 11(a)-(m). The theoretical estimations do not represent the recovery behavior of the material. The average MAPE in recovery for all additive-manufactured samples is 173.15%. It is 1.91 times the MAPE for injection molded one (90.5%).

3.3 Modeling Recovery Using Weibull's Method

The recovery of the samples is modeled using Weibull's Eq 12. When the load is removed, the polymer undergoes instantaneous recovery before the onset viscoelastic recovery process. To model recovery, the instantaneous recovery is first deducted from the total creep just before the load removal. Then, the viscoelastic recovery data are used for the curve fit. Table 6 presents the parameters of Weibull's model determined via the regression analyses.

The Weibull distribution function that governs the recovery of materials depends on the creep load history. The values of the Weibull's recovery parameters change with a change in creep loading. Therefore, a single set of parameters cannot be used universally to characterize the onset viscoelastic recoveries of the samples with different creep load histories. The viscoelastic recovery of each sample is experimentally studied for 1800 s. The Weibull's recovery parameters are determined by fitting the model to the first 900 s recovery data. Then, the model is used to predict the samples' recovery for the next 900 s and beyond, see Fig. 13(a)-(m).

The errors of the recovery strain predictions are calculated. The Weibull's model showed a maximum of 9.61% error for the 0° infill direction and 90% infill density sample. A minimum of 0.22% deviation is found for the 90° infill direction and 90 infill density sample. The injection-molded sample showed a 1.53% error which is half of the 3.61% average error for all additive-manufactured samples. The overall average error of the model is 3.44%, which is more accurate than the Burgers with 173.15%. The big difference in accuracy can be explained by the strain data used to predict the models' parameters. The Burgers model predicts recovery strain using the rheological parameters determined from creep curve fits. However, Weibull's prediction is based on parameters determined by curve fitting the recovery strains. Figure 14 presents the calculated errors of the Weibull's model in recovery strain predictions.

Recent studies on the influences of 3D printing parameters are mostly based on short-term mechanical testing. The influences of infill orientation and moisture content on the tensile strength of additive-manufactured PLA are studied by (Ref 40). The findings indicated that the 90° orientation samples with a 10% moisture content led to optimum tensile strength. A review by Vasile et al. (Ref 41) reported a wide range of findings that discussed the influences of 3D printing parameters on the ultimate tensile strength, izod impact and flexural strength of PLA. The review presented notable variations among the mechanical properties and cited the infill orientation as a primary factor. Generally, alternating + 45°/ − 45° and single 90° infill orientations resulted in better mechanical performances. On the other hand, the influence of infill density on the fracture toughness of PLA is studied using the single edge notch bend (SENB) specimens (Ref 42). For the infill density variations between 10 and 100%, the value of the fracture toughness spans over a wide range. Their findings suggest that the 90% infill density showed the maximum fracture toughness of 2.69MPa$\sqrt{\mathrm{m}}$. The influence of build orientation on the tensile strength and extrapolated fatigue limit at 2×10^6 cycles is studied by (Ref 43). The sample variations were based on vertical, side and horizontal build orientations. Optimum values of 57.15 MPa in tensile strength and 13.5 MPa in fatigue limit were obtained for the horizontal layout. These scholars focus on characterizing the short-term and long-term mechanical properties of PLA and their relations with manufacturing parameters. Regardless, the viscoelastic characterizations of PLA material are areas of limited research, thereby showing the gap.

Our study comprises both experimental and theoretical methods. The experimental studies showed that the creep and

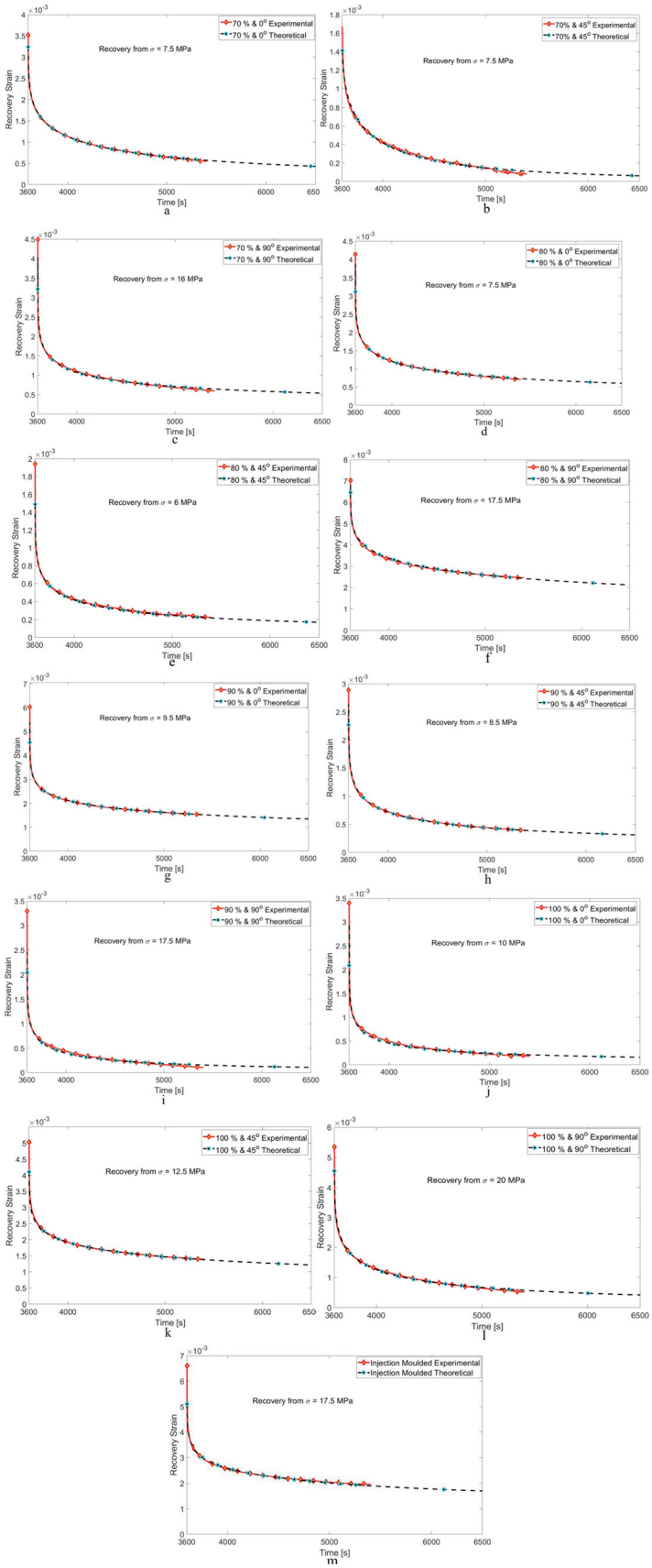
70 % & 0° Experimental
70 % & 0° Theoretical
Recovery from σ = 7.5 MPa
Recovery Strain
Time [s]
a
70% & 45° Experimental
70% & 45° Theoretical
Recovery from σ = 7.5 MPa
Recovery Strain
Time [s]
b
70 % & 90° Experimental
70 % & 90° Theoretical
Recovery from σ = 16 MPa
Recovery Strain
Time [s]
c
80 % & 0° Experimental
80 % & 0° Theoretical
Recovery from σ = 7.5 MPa
Recovery Strain
Time [s]
d
80 % & 45° Experimental
80 % & 45° Theoretical
Recovery from σ = 6 MPa
Recovery Strain
Time [s]
e
80 % & 90° Experimental
80 % & 90° Theoretical
Recovery from σ = 17.5 MPa
Recovery Strain
Time [s]
f
90 % & 0° Experimental
90 % & 0° Theoretical
Recovery from σ = 9.5 MPa
Recovery Strain
Time [s]
g
90 % & 45° Experimental
90 % & 45° Theoretical
Recovery from σ = 8.5 MPa
Recovery Strain
Time [s]
h
90 % & 90° Experimental
90 % & 90° Theoretical
Recovery from σ = 17.5 MPa
Recovery Strain
Time [s]
i
100 % & 0° Experimental
100 % & 0° Theoretical
Recovery from σ = 10 MPa
Recovery Strain
Time [s]
j
100 % & 45° Experimental
100 % & 45° Theoretical
Recovery from σ = 12.5 MPa
Recovery Strain
Time [s]
k
100 % & 90° Experimental
100 % & 90° Theoretical
Recovery from σ = 20 MPa
Recovery Strain
Time [s]
l
Injection Moulded Experimental
Injection Moulded Theoretical
Recovery from σ = 17.5 MPa
Recovery Strain
Time [s]
m

◀**Fig. 13** Curve fitting and predictions of the samples' recovery using Weibull's model for (a) 70% infill density and 0° infill direction, (b) 70% infill density and 45° infill direction, (c) 70% infill density and 90° infill direction, (d) 80% infill density and 0° infill direction, (e) 80% infill density and 45° infill direction, (f) 80% infill density and 90° infill direction, (g) 90% infill density and 0° infill direction (h) 90% infill density and 45° infill direction, (i) 90% infill density and 90° infill direction, (j) 100% infill density and 0° infill direction, (k) 100% infill density and 45° infill direction, (l) 100% infill density and 90% infill direction, (m) injection-molded samples

recovery responses of the injection-molded sample is closely similar to the 90° infill direction for all infill density categories. The injection-molded samples deformed elastically at lower stresses, and recovered the strain fully, see Fig. 9(a) and (b) and Fig. 10(a) and (b). The injection molding process parameters are controlled and optimized during the fill, pack and cooling stages to produce samples with tightly packed molecular chains. The process optimizations improved the viscoelastic behavior of the samples. However, the results of the viscoelastic experiments in Fig. 9(c) and (d) indicated that the creep strains of 90° infill direction samples are slightly better than the injection molded ones. Similarly, in the infill density comparisons, excellent creep resistance behaviors at higher stress loading are found from the 90 and 100% infill densities when their infill direction is at 90°, see Fig. 10(c). The reinforcements in the loading direction and good interlayer adhesions are attributed to the good viscoelastic performances. In this infill direction category, the injection-molded sample is only better than the 70 and 80% infill density variants.

The two theoretical models' creep and recovery predictions provided two different outcomes. The first one indicates that the creep of the tough PLA can be successfully predicted using the Burgers viscoelastic model. Numerous studies used the approach to model the creep of Polyolefin-rubber composite (Ref 19), rubber-graphene composite (Ref 18), fiber-reinforced composite (Ref 13) and PLA blends (Ref 17, 44). Our study showed that the rheological parameters determined by only fitting the creep data cannot be used to obtain reliable predictions of the recovery strain. The reverse approach, where we determine rheological constants by fitting recovery data, did not also produce successful creep predictions. Therefore, we made recovery strain predictions using Weibull's model. The model improved the recovery predictions; however, the values of the parameters in Weibull's model are related to the samples' creep load history. When the creep load changes, the values of the model's recovery parameters change.

FDM additive manufacturing is based on extrusion of the molten polymer through the nozzle, which adds layer after layer during the manufacturing process. In injection molding, the homogenous melt is injected into mold cavities, and the parameters such as injection velocity, packing pressure, and switchover criteria can be regulated during the process. Unlike the injection molding processes, there are no mechanisms to maintain homogenous polymer melt during additive manufacturing. The layer-by-layer filling in FDM also introduces a nonuniform temperature profile that is detrimental to the interlayer adhesions (Ref 6). Print temperature is one of the crucial processing parameters in additive manufacturing. O.Y Gumus et al. (Ref 45) investigated influence of temperature on the mechanical properties of thermoplastic polyurethane manufactured using material extrusion (ME) and compression molding technologies. Within a range of 170- 250°C printing temperature studied, maximum values of 37.6MPa tensile strength and 921% elongation at break were achieved at 230°C. However, our viscoelastic study on tough PLA shows that the 90° infill direction together with optimum infill density can make additive manufacturing compete with conventional injection molding.

4. Conclusions

The creep and recovery behavior of the tough PLA polymer has been studied. We investigated the viscoelastic behavior of the material by varying manufacturing methods and parameters. A total of 13 sample variants were produced using the FDM additive manufacturing injection molding methods. In this paper, we first compared the experimental creep and recovery performances of the additive-manufactured and injection-molded samples. Then, we used two theoretical models (Burgers and Weibull's) to predict the creep and recovery behaviors of the material. Our finds are briefly summarized as follows:

- The viscoelastic deformations of the additive-manufactured samples are highly influenced by infill direction. The comparison of manufacturing methods indicated that superior viscoelastic performances can be obtained from injection-molded samples at lower stress loads. The additive-manufactured samples resist viscoelastic deformation better when the printing parameters are 90° for the infill direction and 90 or 100% for the infill density. These behaviors are observed at higher stress loadings.
- The Burgers viscoelastic model can predict the samples' creep within a linear viscoelastic regime. However, the recovery behavior cannot be predicted with good accuracy. The analyses show that accurate predictions of the samples' recovery cannot be made using the rheological constants determined by curve fitting the creep responses.
- As an effective approach, Weibull's model can be used to predict the recoveries of the samples with pre-specified creep load histories. Weibull's parameters are associated with the creep load histories. When the creep load changes, the recovery parameters in Weibull's equation change.

Previously, we studied the influence of infill patterns on the bending stiffness of PLA beams (Ref 46). We also compared a four elements Maxwell's model with the Burgers to characterize the linear viscoelastic responses of injection-molded Polypropylene (Ref 47). In this paper, we discuss the creep and recovery responses of the tough PLA material. Following this, we will focus on the microstructural analyses of the material undergoing viscoelastic relaxation, nonlinear creep damage and recovery processes.

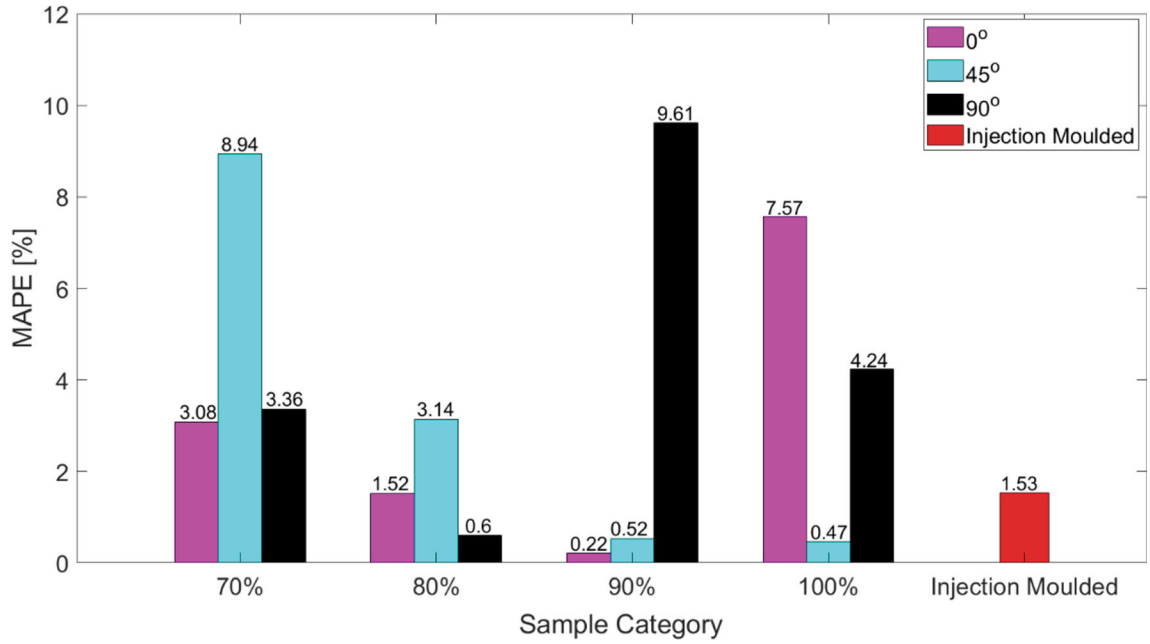

Fig. 14 The mean absolute percentage errors (MAPEs) of Weibull's model in recovery strain predictions for the additive-manufactured and injection-molded samples

Acknowledgment

The authors acknowledge the Mechanical and Sustainable Engineering programme at Arcada University of Applied Sciences for providing access to materials and equipment used in this research.

Open Access

This article is licensed under a Creative Commons Attribution 4.0 International License, which permits use, sharing, adaptation, distribution and reproduction in any medium or format, as long as you give appropriate credit to the original author(s) and the source, provide a link to the Creative Commons licence, and indicate if changes were made. The images or other third party material in this article are included in the article's Creative Commons licence, unless indicated otherwise in a credit line to the material. If material is not included in the article's Creative Commons licence and your intended use is not permitted by statutory regulation or exceeds the permitted use, you will need to obtain permission directly from the copyright holder. To view a copy of this licence, visit http://creativecommons.org/licenses/by/4.0/.

References

1. G. Li, M. Zhao, F. Xu et al., Synthesis and Biological Application of Polylactic Acid, *Molecules*, 2020, **25**(21), p 5023. https://doi.org/10.3390/molecules25215023
2. S. Liu, S. Qin, M. He et al., Current Applications of Poly(Lactic Acid) Composites in Tissue Engineering and Drug Delivery, *Compos. B Eng.*, 2020, **199**, 108238
3. M. Mario, V. Erwin, and C. Andrea, Applications of poly(lactic acid) in commodities and specialties, *Advances in polymer science*. Springer, Cham, 2018
4. S. Farah, D.G. Anderson, and R. Langer, Physical and mechanical properties of PLA, and their functions in widespread applications - A comprehensive review, *Adv. Drug Deliv. Rev.*, 2016, **107**, p 367–392.
5. C. Kaynak and S. Varsavas, Performance Comparison of the 3D-Printed and Injection-Molded PLA and its Elastomer Blend and Fiber Composites, *J. Thermoplast. Compos. Mater.*, 2019, **32**(4), p 501–520.
6. M. Lay, N. Thajudin, Z. Hamid et al., Comparison of physical and mechanical properties of PLA, ABS and nylon 6 fabricated using fused deposition modeling and injection molding, *Compos. B Eng.*, 2019, **176**, 107341
7. M. Hsueh, C. Lai, S. Wang et al., Effect of Printing Parameters on the Thermal and Mechanical Properties of 3D-Printed PLA and PETG, Using Fused Deposition Modeling, *Polymers*, 2021, **13**(14), p 2387. https://doi.org/10.3390/polym13142387
8. M. Hsueh, C. Lai, C. Chung et al., Effect of Printing Parameters on the Tensile Properties of 3D-Printed Polylactic Acid (PLA) Based on Fused Deposition Modeling, *Polymers*, 2021, **13**, p 2387. https://doi.org/10.3390/polym13142387
9. M. Algarni, The Influence of Raster Angle and Moisture Content on the Mechanical Properties of PLA Parts Produced by Fused Deposition Modeling, *Polymers*, 2021, **13**, p 237. https://doi.org/10.3390/polym13020237
10. T. Yao, J. Ye, Z. Deng et al., Tensile Failure Strength and Separation Angle of FDM 3D Printing PLA Material: Experimental and theoretical analyses, *Compos. B Eng.*, 2020, **188**, 107894
11. M. Caminero, J. Chacón, E. García-Plaza et al., Additive Manufacturing of PLA-Based Composites Using Fused Filament Fabrication: Effect of Graphene Nanoplatelet Reinforcement on Mechanical Properties, Dimensional Accuracy and Texture, *Polymers*, 2019, **11**(5), p 799. https://doi.org/10.3390/polym11050799
12. M. Feven, K. Mohammad, R. Gunasunderi et al., Viscoelastic Properties and Thermal Stability of Nanohydroxyapatite Reinforced Poly-Lactic Acid for Load Bearing Applications, *Molecules*, 2021, **26**(19), p 5852. https://doi.org/10.3390/molecules26195852
13. R. Ans and K. Muammer, Creep and Recovery Behavior of Continuous Fiber-Reinforced 3DP Composites, *Polymers*, 2021, **13**(10), p 1644. https://doi.org/10.3390/polym13101644
14. P. Reis, S. Valves, and J. Ferreira, Creep and Stress Relaxation Behaviour of 3D Printed Nanocomposites: Creep and Stress Relaxation Behaviour of 3D Printed Nanocomposites, *Proc. Struct. Integr.*, 2022, **37**, p 934–940.
15. M. Morreale, M. Mistretta, and V. Fiore, Creep Behavior of Poly(lactic acid) Based Biocomposites, *Materials*, 2017, **10**(4), p 395. https://doi.org/10.3390/ma10040395

16. T. Tezel, V. Kovan, and E. Topal, Effects of the Printing Parameters on Short-Term Creep Behaviors of Three-Dimensional Printed Polymers, *J. Appl. Polym. Sci.*, 2019, **136**(21), p 47564.
17. J. Ye, T. Yao, Z. Deng et al., A Modified Creep Model of Polylactic Acid (PLA-max) Materials with Different Printing Angles Processed by Fused Filament Fabrication, *J. Appl. Polym.*, 2021, **138**(17), p 50270.
18. C. Xue, H. Gao, Y. Hu, and G. Hu, Experimental Test and Curve Fitting of Creep Recovery Characteristics of Modified Graphene Oxide Natural Rubber and its Relationship with Temperature, *Polym. Test.*, 2020, **87**, p 106509.
19. F. Daver, M. Kajtaz, M. Brandt, and R. Shanks, Creep and Recovery Behaviour of Polyolefin-Rubber Nanocomposites Developed for Additive Manufacturing, *Polymers*, 2016, **8**(12), p 437. https://doi.org/10.3390/polym8120437
20. D. Garlotta, A Literature Review of Poly(Lactic Acid), *J. Polym. Environ.*, 2001, **9**, p 63–84.
21. T. Casalini, F. Rossi, A. Castrovinci, and G. Perale, A Perspective on Polylactic Acid-Based Polymers Use for Nanoparticles Synthesis and Applications, *Front. Bioeng. Biotechnol.*, 2019, **7**, p 259.
22. M.S. Singhvi, S.S. Zinjarde, and D.V. Gokhale, Polylactic Acid: Synthesis and Biomedical Applications, *J. Appl. Microbiol.*, 2019, **127**(6), p 1612–1626. https://doi.org/10.1111/jam.14290
23. Go Beyond Concept Modeling: Create Functional Prototypes with MakerBot Tough PLA, MakerBot Industries. https://www.makerbot.com/stories/design/go-beyond-concept-modeling-create-functional-durable-prototypes-and-parts-with-makerbot-tough-pla/ [Accessed: Sept. 1, 2022]
24. Reasons to choose Ultimaker Tough PLA, Ultimaker. https://ultimaker.com/materials/tough-pla [Accessed: Aug. 23,2022]
25. Biocompounds for Industrial Applications, BIO-FED. https://bio-fed.com/ [Accessed: June 12, 2022]
26. DATA SHEET, colorFabb, https://colorfabb.com/data-sheets [Accessed: May 25, 2022]
27. User manual: Guideline for NC5 plus controller, Simutomo-Demag, http://onlinestore.dpg.com/intelectmain.html [Accessed: June 13, 2022]
28. G. Menges, W. Michaeli, and P. Mohren, *How to make injection molds*, Carl Hanser Verlag, Munich, 2001, p 271–333
29. W.N. Findley, J.S. Lai, and K. Onaran, *Creep and relaxation of nonlinear viscoelastic materials with an introduction to linear viscoelasticity*, Dover Publications, New York, 1978
30. U.W. Gedde, M.S. Hedenqvist, M. Hakkarainen, F. Nilsson, and O. Das, Mechanical properties, *Applied polymer science*. Springer, Cham, 2021
31. R. Lakes, Constitutive relations, *Viscoelastic materials*. Cambridge University Press, Cambridge, 2010, p 14–54
32. J. Bergström, Linear viscoelasticity, *Mechanics of solid polymers*. William Andrew Publishing, 2015, p 309–351
33. J.D. Ferry, *Viscoelastic properties of polymers*, Wiley, 1980
34. D. Gutierrez-Lemini, *Engineering viscoelasticity*, Springer, New York, 2001
35. R.J. Crawford and P.J. Martin, *Plastics engineering*, 4th ed. Elsevier, Hampshire, 2020, p 59–194
36. E. Riande, R. Diaz-Calleja, M. Prolongo et al., *Polymer viscoelasticity stress and strain in practice*, Marcel Dekker, New York, 1999
37. S.K. Fancey, A Latch-Based Weibull Model for Polymerie Creep and Recovery, *J. Polym. Eng.*, 2001, **21**(6), p 489–510.
38. S.K. Fancey, A Mechanical Model for Creep, Recovery and Stress Relaxation in Polymeric Materials, *J. Mater. Sci.*, 2005, **40**, p 4827–4831. https://doi.org/10.1007/s10853-005-2020-x
39. S. Kim and H. Kim, A new metric of absolute percentage error for intermittent demand forecasts, *Int. J. Forecast.*, 2016, **32**(3), p 669–679.
40. M. Algarni, The Influence of Raster Angle and Moisture Content on the Mechanical Properties of PLA Parts Produced by Fused Deposition Modeling, *Polymers*, 2021, **13**(2), p 237.
41. V. Cojocaru, D. Frunzaverde, C.-O. Miclosina, and G. Marginean, The Influence of the Process Parameters on the Mechanical Properties of PLA Specimens Produced by Fused Filament Fabrication—A Review, *Polymers*, 2022, **14**(5), p 886.
42. A. Milovanović, Z. Golubović, I. Trajković et al., Influence of Printing Parameters on the Eligibility of Plane-Strain Fracture Toughness Results for PLA Polymer, *Proc. Struct. Integr.*, 2022, **41**, p 290–297.
43. G. Morettini, M. Palmieri, L. Capponi et al., Comprehensive Characterization of Mechanical and Physical Properties of PLA Structures Printed by FFF-3D-Printing Process in Different Directions, *Prog. Addit. Manuf.*, 2022, **7**, p 1111–1122. https://doi.org/10.1007/s40964-022-00285-8
44. Y.-S. Jhao, H. Ouyang, F. Yang, and S. Lee, Thermo-Mechanical and Creep Behaviour of Polylactic Acid/Thermoplastic Polyurethane Blends, *Polymers*, 2022, **14**, p 5276. https://doi.org/10.3390/polym14235276
45. O.Y. Gumus, R. Ilhan, and B.E. Canli, Effect of Printing Temperature on Mechanical and Viscoelastic Properties of Ultra-flexible Thermoplastic Polyurethane in Material Extrusion Additive Manufacturing, *J. Mater. Eng. Perform.*, 2022, **31**, p 3679–3687.
46. S.Z. Gebrehiwot, L. Espinosa Leal, J.N. Eickhoff et al., The Influence of Stiffener Geometry on Flexural Properties of 3D Printed Polylactic Acid (PLA) Beams, *Prog. Addit. Manuf.*, 2021, **6**, p 71–81. https://doi.org/10.1007/s40964-020-00146-2
47. S.Z. Gebrehiwot and L. Espinosa-Leal, Characterising the Linear Viscoelastic Behaviour of an Injection Moulding Grade Polypropylene Polymer, *Mech. Time Depend. Mater.*, 2021 https://doi.org/10.1007/s11043-021-09513-0

Publisher's Note Springer Nature remains neutral with regard to jurisdictional claims in published maps and institutional affiliations.